

Article

Geochemical Features of Lacustrine Shales in the Upper Cretaceous Qingshankou Formation of Changling Sag, Songliao Basin, Northeast China

Zhongcheng Li ^{1,2,3}, Zhidong Bao ^{2,3}, Zhaosheng Wei ¹, Lei Li ^{2,3} and Hailong Wang ^{1,*}

¹ Research Institute of Exploration and Development, PetroChina Jilin Oilfield Company, Songyuan 138000, China

² College of Geosciences, China University of Petroleum-Beijing, Beijing 102249, China

³ State Key Laboratory of Petroleum Resource and Prospecting, China University of Petroleum-Beijing, Beijing 102249, China

* Correspondence: wanghl-jlyt@petrochina.com.cn

Abstract: The organic-rich shale of the Upper Cretaceous Qingshankou Formation is an important hydrocarbon source rock in Northeast China. In this study, taking the lacustrine shale in the Qingshankou Formation as an example, geochemical analysis, including total organic carbon (TOC), Rock-Eval pyrolysis, maceral compositions, X-ray diffraction (XRD), and biomarker analyses, were carried out on twenty-four shale samples to evaluate the geochemistry and environmental features of this shales. The Qingshankou lacustrine shales contains mainly Type I/II₁ organic matter and is oil prone, with a good to excellent source rock. Vitrinite reflectance and Rock-Eval pyrolysis parameters show that the Qingshankou lacustrine shales is mainly in the mature stage and within the oil window. Biomarker composition of the shales provide evidence that the Qingshankou lacustrine shales was formed in a reductive sedimentary environment with relatively high salinity water. The organic matter came from a mixture of plankton, bacterial and land plants.

Keywords: geochemical features; paleoenvironment; shale oil; Qingshankou Formation; Changling sag; Songliao Basin



Citation: Li, Z.; Bao, Z.; Wei, Z.; Li, L.; Wang, H. Geochemical Features of Lacustrine Shales in the Upper Cretaceous Qingshankou Formation of Changling Sag, Songliao Basin, Northeast China. *Energies* **2022**, *15*, 6983. <https://doi.org/10.3390/en15196983>

Academic Editors: Bei Liu, Tian Dong, Wenhao Li, Kun Jiao and Zhen Qiu

Received: 23 June 2022

Accepted: 28 August 2022

Published: 23 September 2022

Publisher's Note: MDPI stays neutral with regard to jurisdictional claims in published maps and institutional affiliations.



Copyright: © 2022 by the authors. Licensee MDPI, Basel, Switzerland. This article is an open access article distributed under the terms and conditions of the Creative Commons Attribution (CC BY) license (<https://creativecommons.org/licenses/by/4.0/>).

1. Introduction

With the constant increase in energy demand and exhaustion of conventional oil and gas resources, unconventional energy resources have drawn wide attention. Due to very low production, shale oil was not taken seriously in the past. Nevertheless, following the successful commercial development of shale gas in North America, shale oil exploration developed rapidly worldwide [1].

Shale oil refers to oil accumulating in shale layers or interlayers (sandstone, dolomite, limestone, and tuff) associated with shale [2]. It forms a type of self-sourcing reservoir and exists in an adsorption state or in a free state, existing in micro- and nano-scaled pores and fractures [3]. This leads to common issues such as low production and fast decline during the development of shale oil, making it difficult to develop and be economically viable on a large scale. Natural or artificial fracture is a main factor controlling the high production of shale oil.

Shale oil resources are widespread throughout China, such as the Middle Permian Lucaogou Formation in Santanghu Basin in northwest China, the Paleogene Shahejie Formation in various depressions in the Bohai Bay Basin, the Upper Cretaceous Qingshankou and Nenjiang formations in Songliao Basin in northeast China, the Eocene Hetaoyuan Formation in Biyang Depression Nanxiang Basin in the middle eastern part of China, and the Cenozoic Qianjiang Formation of the Jiangnan Basin [2,4–8].

As a source rock, organic-rich shale plays a vital role in the process of hydrocarbon generation [9,10]. Hydrocarbon generation potentials are affected by the quality of source

rock to a large extent. Sedimentary environment and preservation conditions control the abundance, type, and thermal evolution of organic matter. Organic matter maceral, vitrinite reflectance, total organic matter (TOC), rock pyrolysis parameters, element contents, and molecular geochemical parameters are often used to evaluate the hydrocarbon generation potential of shale.

Different from marine shale, lacustrine shale layers are often strongly heterogeneous, as continental faulted lake basins often have gone through complex tectonic evolution during geologic history and have large scale fault systems [11,12]. To evaluate oil and gas resource potentials accurately, it is necessary to examine the geochemical and sedimentary environment features of the region of interest in detail.

Numerous studies have focused on the organic–inorganic characteristics, origin, and accumulation of organic matter within Cretaceous black shales [13–16]. However, these studies are mainly concentrated in the northern region of the basin, lacking systematic research in the southern region of the basin. Therefore, based on a series of geochemical and biomarker analysis experiments, the goal of this study was to present a more comprehensive understanding of the chemistry of the region in addition to sedimentary environment information in order to provide useful information for the prediction of shale oil’s “sweet spot”.

2. Geologic Setting

Located in northeastern China, Songliao Basin is a continental sedimentary basin formed in the Mesozoic–Cenozoic era. Structurally, it consists of six first order structural units: central depression, west slope, southwest uplift, southeast uplift, northeast uplift, and north subduction zone (Figure 1).

The tectonic evolution of the basin can be divided into three stages: fault depression, depression, and structural inversion. The depositional period of the Lower Cretaceous Huoshiling, Shahezi, and Yingcheng formations was the fault depression stage of the lake basin. The depositional period of the Lower Cretaceous Denglouku Formation is the transition stage between fault depression and depression. The depositional period of the Lower Cretaceous Quantou Formation and Upper Cretaceous Qingshankou, Yaojia, Nengjiang, Sifangtai, and Mingshui formations is the depression stage of the lake basin. In the initial depositional stage of the Upper Cretaceous Qingshankou Formation, the climate was warm and humid, the lake water was deep, and the lake basin expanded rapidly. Consequently, a succession of black/gray mudstone interbedded with gray siltstone and ostracoda-bearing limestone developed. The Qingshankou Formation is divided into three members, Qing 1, Qing 2, and Qing 3, from the bottom up. The depositional period of Qing 1 was the largest lake transgression period, when a set of deep-lake black shale with Type I and II 1 organic matter and good hydrocarbon generation potential deposited [17]. The study area, Jilin oilfield, is located in the southern part of Songliao Basin next to the Daqing oilfield to the north, where the target layer series, Cretaceous Qingshankou Formation, has massive lacustrine shale development.

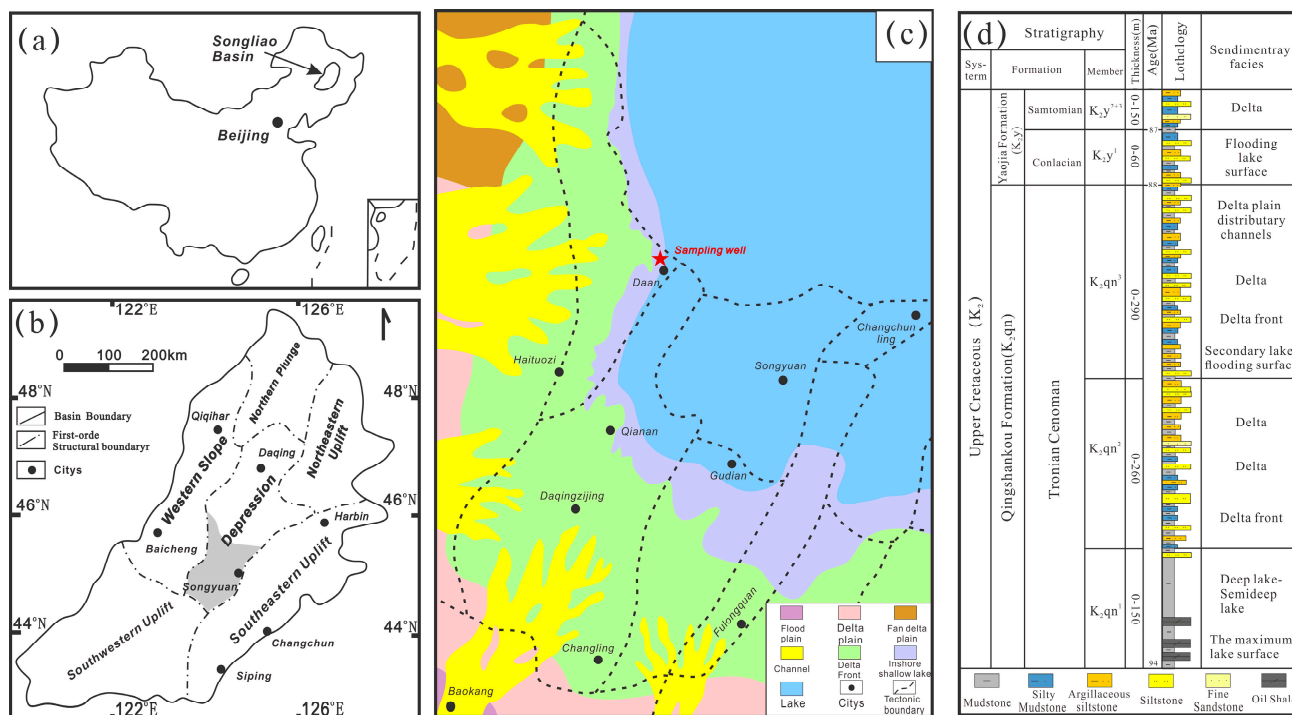


Figure 1. (a) Location of Songliao Basin in China; (b) six tectonic units of Songliao Basin; (c) location of the study area in Songliao Basin; (d) stratigraphic column and lithology of the Qingshankou Formation in Songliao Basin (Adapted from Refs. [6,18]).

3. Samples and Experiments Methods

3.1. Samples

A total of twenty-four shale samples for experiments were taken from the Upper Cretaceous Qingshankou Formation in Changling sag, southern Songliao Basin (Figure 1).

3.2. Experimental Methods

The device for the TOC test was a C-744 carbon sulfur analyzer, and the experiment process follows GB/T 19145-2003 “Test of TOC in sedimentary rocks”. Before the experiment, the samples were ground into a hundred mesh in agate mortar, and diluted hydrochloric acid was then added to react with the sample to remove inorganic carbonates. The remaining sample was washed with water and dried, and then calcined to obtain CO₂ and SO₂; finally, the TOC and total sulfur content were tested using a thermal conductivity detector. The device for the pyrolysis experiment was a French Rock-Eval-6plus source rock analyzer, and the experimental process was followed by GB/T 18602-2012 “Rock Pyrolysis Analysis”. The XRD experimental instrument was a D8 discovery X-ray diffractometer, and the experiment process was followed by SY/T 5163-2010. The saturated hydrocarbon chromatography-mass spectrometry experiment adopted extraction under room temperature methods. The shale sample was soaked in dichloromethane solution and then set aside for 12 h, after which the extraction fluid was analyzed by an HP7890 chromatograph. The experiment process abided by SY/T 5779-2008: “Analytical method of hydrocarbons in petroleum and sediment by chromatography”.

4. Results and Discussion

4.1. Mineral Compositions and Lithofacies Classification

The mineral composition determined by XRD of lacustrine shale in Qingshankou Formation comprised mainly quartz, feldspar, and clay (Figure 2, Table 1). The content of quartz was between 23.6 and 41.0%, with an average of 31.9%. The feldspar content was between 12.4 and 30.2%, with an average of 19.3%. The clay mineral content was

the highest, ranging from 23.3 to 42.4%, with an average of 35.8%. Clay minerals were mainly illite, with a relative average content of 76.0%, followed by a mixed layer of illite–smectite (with a relative average content of 16.3%) and a small amount of chlorite (with a relative average content of 7.7%). The average content of other minerals was less than 10%. According to the average content, they are calcite (5.8%), pyrite (3.9%), iron dolomite (2.5%), and siderite (0.8%).

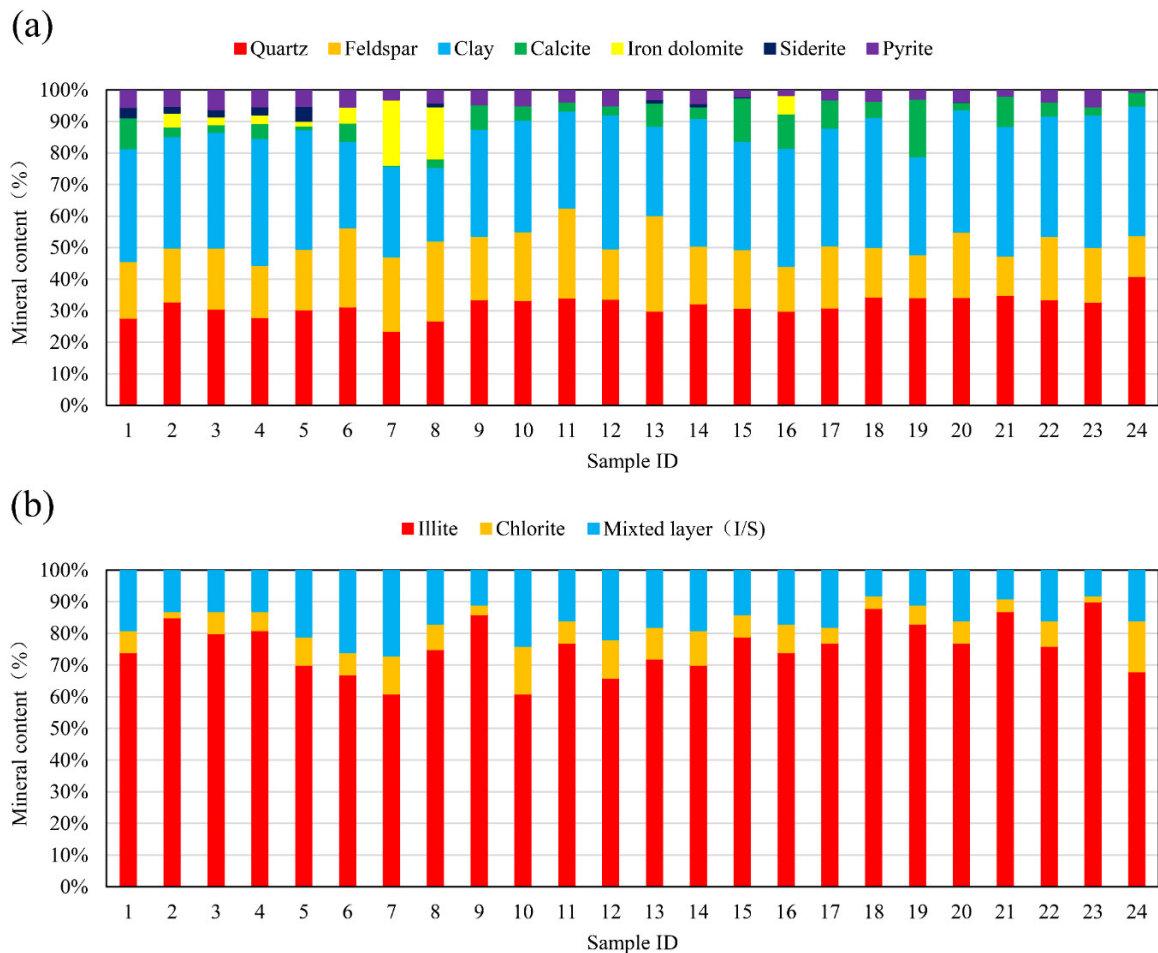


Figure 2. Histograms of the mineral composition of Qingshankou lacustrine shale samples. (a) Whole rock mineral compositions; (b) Clay mineral compositions.

Based on the ternary graph of the content of the siliceous minerals (quartz and feldspar), carbonate minerals, and clay minerals [19–21], it was demonstrated that Qingshankou shales can mainly be classified into two types: argillaceous/siliceous mixed shale lithofacies (M-2) and clay-rich siliceous shale lithofacies (S-3) (Figure 3, Table 1).

Table 1. Mineralogical compositions and lithofacies of Qingshankou Formation shales.

Sample ID	Depth	Quartz	Feldspar	Calcite	Iron Dolomite	Siderite	Pyrite	Clay	Illite	Chlorite	Mixed Layer (I/S)	Lithology
1	1971.2	27.7	18	9.7		3.3	5.5	35.8	74	7	19	M-2
2	1976.9	32.9	17	3.1	4.4	2.1	5.2	35.3	85	2	13	M-2
3	1979.6	30.6	19.3	2.4	2.5	2.3	6.2	36.7	80	7	13	M-2
4	1982.2	27.9	16.5	4.7	2.7	2.6	5.3	40.2	81	6	13	M-2
5	1984.3	30.4	19.2	1.2	1.5	4.7	5.2	37.9	70	9	21	M-2
6	2001.8	31.3	25	5.7	5.1		5.4	27.5	67	7	26	S-3
7	2003.7	23.6	23.5	0.3	20.7		3.1	28.8	61	12	27	M-2
8	2009.7	26.9	25.3	2.7	16.5	1.2	4.1	23.3	75	8	17	S-2
9	2011.9	33.5	20.1	7.7			4.7	34	86	3	11	S-3
10	2014.6	33.4	21.7	4.5			5	35.4	61	15	24	S-3
11	2016.2	34.1	28.5	2.9			3.8	30.7	77	7	16	S-3

Table 1. Cont.

Sample ID	Depth	Quartz	Feldspar	Calcite	Iron Dolomite	Siderite	Pyrite	Clay	Illite	Chlorite	Mixed Layer (I/S)	Lithology
12	2017.8	33.7	16	2.9			5	42.4	66	12	22	M-2
13	2025.5	30	30.2	7.3		1.1	3	28.4	72	10	18	S-3
14	2030.5	32.3	18.3	3.7		1	4.3	40.4	70	11	19	S-3
15	2033.3	30.9	18.5	13.7		0.4	2.1	34.4	79	7	14	M-2
16	2035.6	30	14.2	10.9	5.8		1.7	37.5	74	9	17	M-2
17	2038.0	30.9	19.7	9			3.1	37.2	77	5	18	S-3
18	2042.8	34.5	15.7	5			3.6	41.3	88	4	8	S-3
19	2044.3	34.2	13.6	18.2			2.9	31.1	83	6	11	M-2
20	2046.5	34.3	20.7	2.4		0.2	3.7	38.7	77	7	16	S-3
21	2048.2	35	12.4	9.6			1.9	41.1	87	4	9	M-2
22	2051.3	33.5	20.1	4.5			3.7	38.2	76	8	16	S-3
23	2055.0	32.8	17.4	2.6			5.3	41.9	90	2	8	S-3
24	2062.6	41	12.9	4.5			0.6	41	68	16	16	S-3

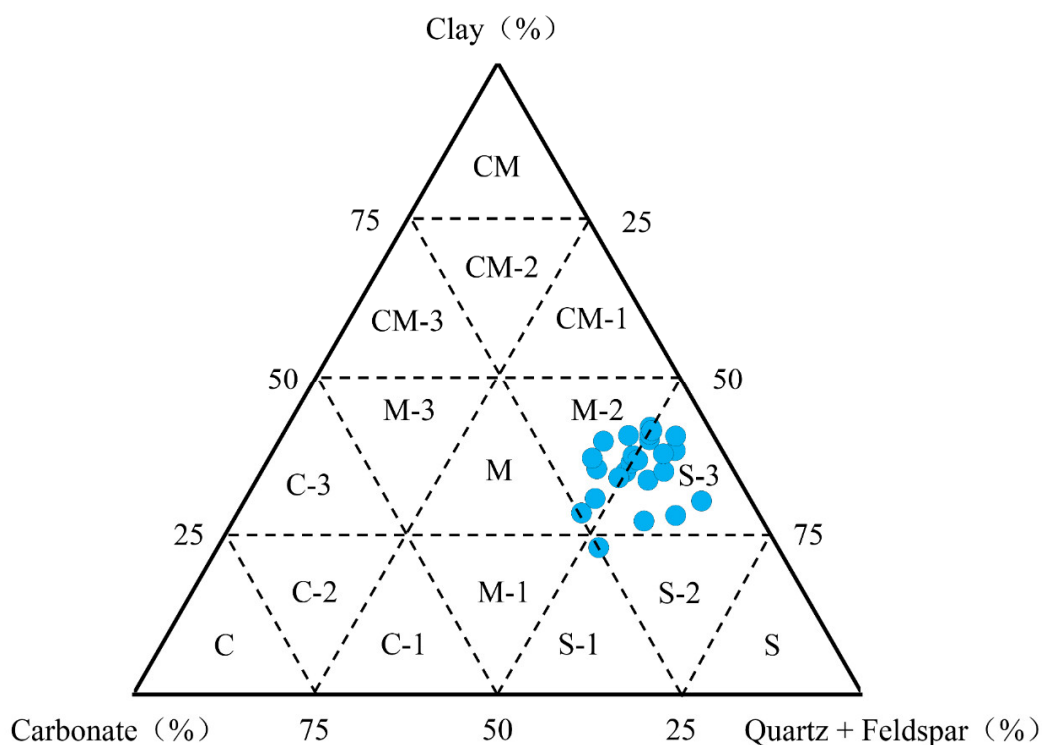


Figure 3. Classification of shale lithofacies in the study area (Adapted from Refs. [19–21]). S: Siliceous shale lithofacies; S-1: Carbonate-rich siliceous shale lithofacies; S-2: Mixed siliceous shale lithofacies; S-3: Clay-rich siliceous shale lithofacies; M: Mixed shale lithofacies; M-1: Calcareous/siliceous mixed shale lithofacies; M-2: Argillaceous/siliceous mixed shale lithofacies; M-3: Argillaceous/calcareous mixed shale lithofacies; CM: Argillaceous shale lithofacies; CM-1: Silica-rich argillaceous shale lithofacies; CM-2: Mixed argillaceous shale lithofacies; CM-3: Carbonate-rich argillaceous shale lithofacies.

4.2. Organic Geochemical Characteristics

4.2.1. Organic Matter Abundance

Parameters commonly used to evaluate the abundance of organic matter in source rocks include TOC and $(S_1 + S_2)$ [22,23].

According to a TOC of less than 0.5%, 0.5–1%, 1–2% and greater than 2%, and $(S_1 + S_2)$ of less than 3 mg/g, 3–6 mg/g, 6–20 mg/g, and greater than 20 mg/g, shale can be classified into four grades: poor, average, good, and excellent [24,25]. As shown in Table 2, TOC range from 1.40% to 2.78% (2.01% on average), S_1 range from 1.22 mg/g to 2.85 mg/g (2.06 mg/g on average), S_2 range from 5.56 mg/g to 13.42 mg/g (10.25 mg/g on average), and $S_1 + S_2$ range from 7.11 mg/g to 15.79 mg/g (12.30 mg/g on average). Figure 4 shows the cross-plot of TOC vs. $(S_1 + S_2)$. It can be seen from Figure 4 that all shale samples fall in the zones of “good” and “excellent”.

Table 2. Statistics of geochemical biomarker parameters of the Qingshankou lacustrine shales.

Sample ID	Depth	TOC	S ₁	S ₂	S ₁ + S ₂	S ₁ /(S ₁ + S ₂)	HI	OI	T _{max}	Ro	CPI	C _{27st} %	C _{28st} %	C _{29st} %	(G/C ₃₀ H)	(Pr/Ph)	Ph/nC18	Pr/nC17
1	1971.2	1.94	1.57	13.42	14.99	0.10	693	0.64	446	1.01	1.14	27.78	19.88	52.34	0.34	0.89	0.10	0.10
2	1976.9	1.40	1.43	8.17	9.60	0.15	584	0.57	447	1.03	1.10	28.54	21.20	50.26	0.37	0.96	0.10	0.10
3	1979.6	1.78	1.96	12.76	14.72	0.13	718	0.69	448	1.05	1.09	30.71	21.48	47.81	0.34	0.99	0.10	0.11
4	1982.2	1.82	1.82	10.54	12.36	0.15	580	0.57	447	1.08	1.09	26.52	28.13	45.34	0.56	0.77	0.10	0.01
5	1984.3	1.79	1.76	9.79	11.55	0.15	547	0.54	445	1.07	1.09	29.72	23.97	46.32	0.50	0.88	0.12	0.10
6	2001.8	1.46	2.13	7.42	9.55	0.22	510	0.54	440	1.04	1.11	30.31	25.01	44.68	0.45	1.15	0.14	0.18
7	2003.7	2.66	1.83	12.67	14.50	0.13	476	0.45	453	1.07	1.11	31.61	23.90	44.49	0.49	0.94	0.14	0.15
8	2009.7	1.48	2.27	7.08	9.35	0.24	478	0.53	445	1.01	1.10	29.95	23.42	46.62	0.51	0.71	0.20	0.16
9	2011.9	1.66	1.55	5.56	7.11	0.22	335	0.36	451	1.08	1.12	29.94	23.32	46.74	0.43	1.32	0.21	0.26
10	2014.6	2.06	2.18	11.66	13.84	0.16	566	0.56	447	1.07	1.12	32.52	22.26	45.22	0.48	1.21	0.15	0.19
11	2016.2	2.78	2.14	12.08	14.22	0.15	435	0.43	454	1.08	1.11	29.69	23.26	47.05	0.48	1.07	0.19	0.21
12	2017.8	1.99	2.07	10.36	12.43	0.17	522	0.52	443	1.08	1.12	29.87	22.85	47.28	0.37	1.13	0.19	0.21
13	2025.5	2.05	2.41	9.10	11.51	0.21	444	0.47	446	1.07	1.17	28.58	25.43	45.98	0.38	1.05	0.20	0.22
14	2030.5	2.02	2.14	10.49	12.63	0.17	519	0.52	449	1.10	1.12	32.10	21.74	46.16	0.31	0.78	0.18	0.16
15	2033.3	2.33	2.42	9.64	12.06	0.20	414	0.43	450	1.07	1.10	29.48	21.71	48.80	0.39	1.09	0.18	0.20
16	2035.6	2.03	2.82	9.06	11.88	0.24	446	0.49	435	1.09	1.11	30.67	22.16	47.17	0.37	1.22	0.20	0.24
17	2038.0	2.38	2.16	10.46	12.62	0.17	440	0.44	453	1.05	1.10	29.89	22.44	47.67	0.35	1.28	0.14	0.17
18	2042.8	2.20	2.85	11.71	14.56	0.20	533	0.55	452	1.07	1.08	35.17	23.14	41.69	0.39	0.97	0.17	0.16
19	2044.3	1.66	1.70	8.41	10.11	0.17	508	0.51	452	1.11	1.09	31.23	22.13	46.65	0.34	1.13	0.11	0.13
20	2046.5	2.00	1.83	11.07	12.90	0.14	554	0.54	451	1.12	1.10	27.54	24.11	48.35	0.37	1.14	0.14	0.17
21	2048.2	2.11	2.11	12.48	14.59	0.14	593	0.57	452	1.05	1.14	32.71	21.87	45.42	0.36	0.91	0.12	0.11
22	2051.3	2.38	2.52	11.79	14.31	0.18	496	0.50	452	1.10	1.20	33.23	21.99	44.79	0.33	1.11	0.12	0.14
23	2055.0	1.55	1.22	6.90	8.12	0.15	445	0.43	451	1.07	1.17	32.01	21.56	46.43	0.34	1.13	0.11	0.13
24	2062.6	2.68	2.44	13.35	15.79	0.15	498	0.49	459	1.06	1.17	33.20	22.24	44.56	0.43	1.05	0.12	0.12

T_{max} = temperature at which maximum hydrocarbon generation (°C); TOC = total organic carbon (weight percent wt% of the whole rock); S₁ = volatile hydrocarbon content (mg hydrocarbon/g rock); S₂ = remaining hydrocarbon content (mg hydrocarbon/g rock); HI = hydrogen index (mg S₂/g TOC); OI = oxygen index (mg S₃/g TOC).

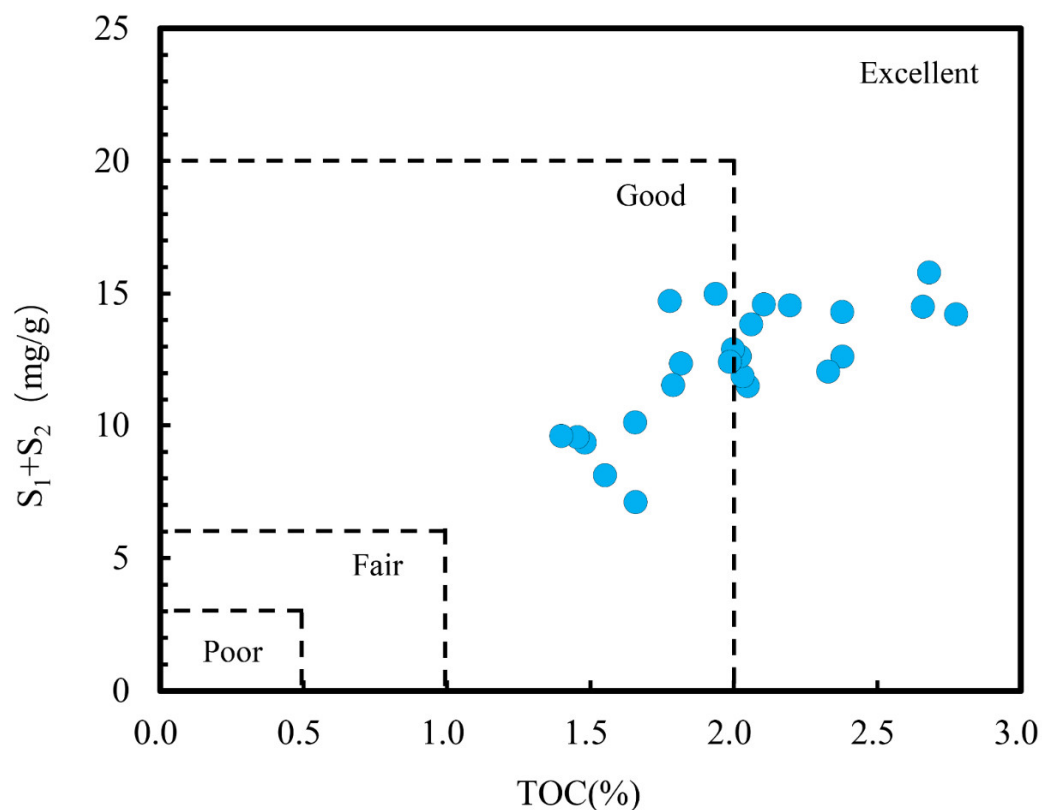


Figure 4. Diagram of TOC vs. ($S_1 + S_2$) (Adapted from Ref. [24]).

4.2.2. Types of Organic Matter

The type of organic matter determines the oil prone or gas prone of source rock [23]. Rock-Eval pyrolysis parameters can be used to evaluate the types of organic matter in shale. Nevertheless, Rock-Eval pyrolysis parameters may be affected in some cases due to mineralogical compositions and certain kerogens [26–32]. Therefore, it is necessary to use a variety of experimental parameters to study the types of organic matter.

The HI vs. T_{max} diagram shows that the organic matter in the Qingshankou lacustrine shales is types I and II₁, suggesting an oil prone of organic matter (Figure 5).

The S_2 vs. TOC diagram can also be used to identify organic matter types [33]. The slope of the S_2 -TOC curve denotes the hydrogen index HI ($HI = S_2/TOC$). An HI of less than 50 mg/g, 50–200 mg/g, 200–300 mg/g, 300–600 mg/g, and greater than 600 mg/g denotes Type I (continental, oil prone), II (marine, oil prone), II/III (oil and gas prone), III (gas prone), and IV (dry gas prone) [34]. According to the above standard, the shale samples from the Qingshankou Formation mainly comprise Type II and partial Type I kerogen, indicating that they have oil-generation potentials (Figure 6).

The maceral composition of the shale samples can also be applied to the determination of kerogen types [35,36]. The compositions of the organic macerals of the Qingshankou lacustrine shales are shown in Figure 7 and Table 3. The ternary diagram of maceral groups indicates that the sapropelinite is the dominant component, which is favorable for oil generation, with the range from 80.6 to 88.9 vol %, and averaged 85.4 vol %, followed by vitrinite (5.0–12.4 vol %; average: 7.5 vol %) and inertinite (3.1–11.2 vol %; average: 5.9 vol %), the abundance of the liptinite is very low (1.0–1.7 vol %, average: 1.2 vol %). The type index of organic matter (TI) can be used to distinguish organic matter type. All samples fall into the type I (two samples) and II₁ (seventeen samples) category.

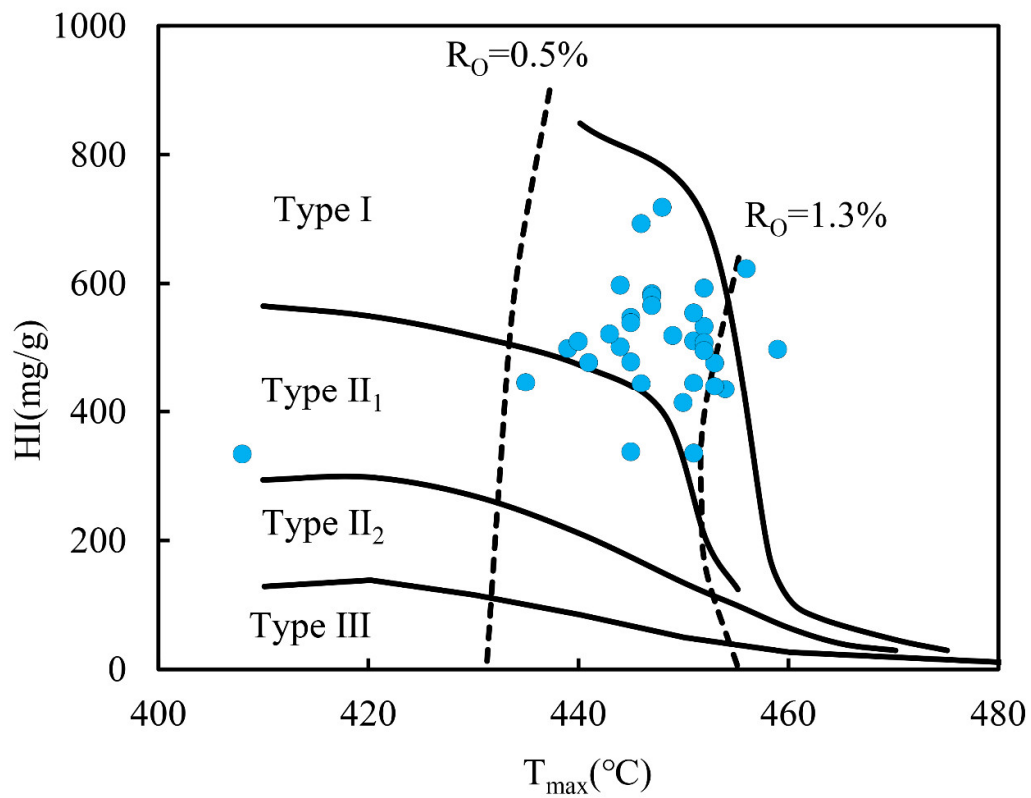


Figure 5. Diagram of HI vs. T_{max} , indicating types I and II₁ organic matter of the Qingshankou lacustrine shales.

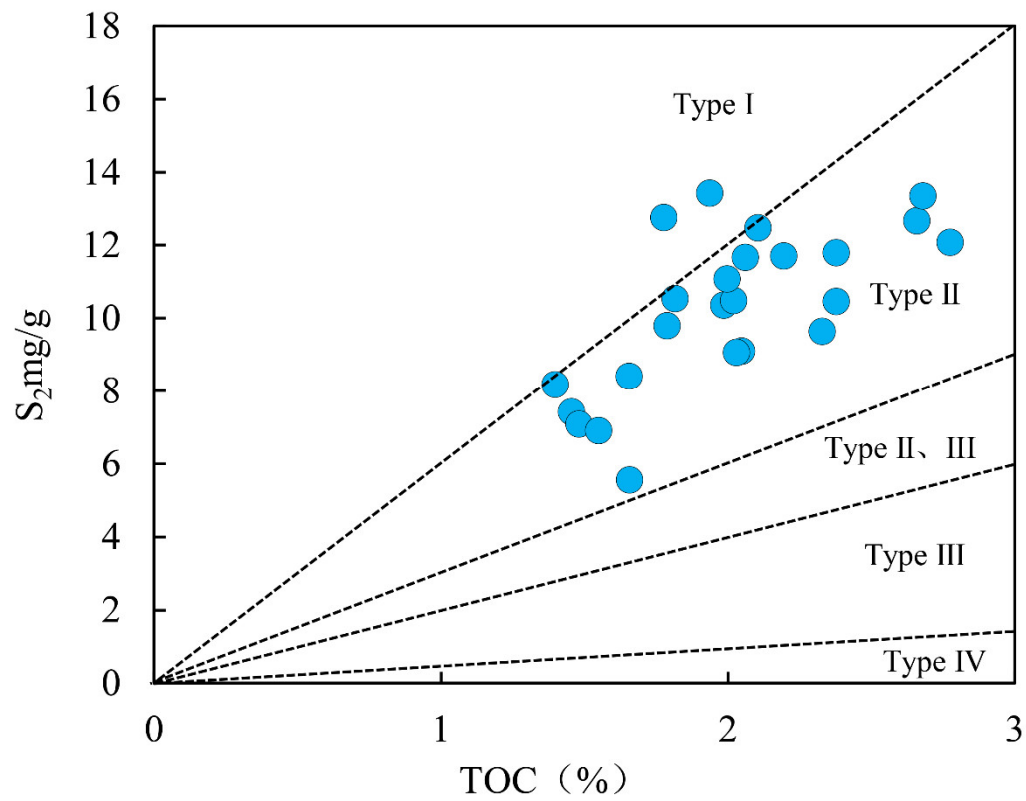


Figure 6. Diagram of S_2 vs. TOC, indicating types I and II organic matter of the Qingshankou lacustrine shales.

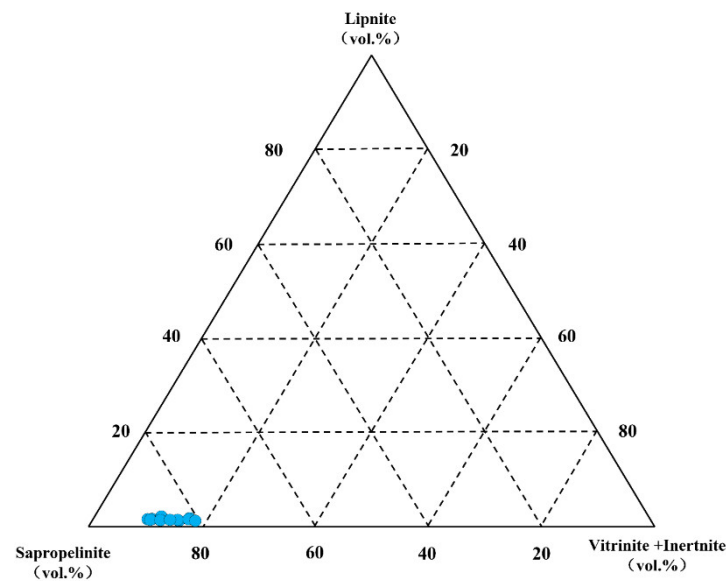


Figure 7. Ternary diagram of maceral composition for kerogen-type identification showing the dominance of sapropelinite and Type I and II₁ kerogen.

Table 3. Composition of organic macerals of the Qingshankou lacustrine shales.

Sample ID	Depth (m)	Sapropelinite (%)	Liptinite (%)	Vitrinite (%)	Inertinite (%)	TI	Type
1	1971.18	81.3	1.3	9.3	8.0	67.0	II1
2	1976.86	81.4	1.4	10.0	7.1	67.5	II1
3	1979.55	87.1	1.1	6.5	5.4	77.4	II1
4	1982.21	84.8	1.0	7.1	7.1	73.0	II1
5	1984.25	86.5	1.0	8.3	4.2	76.6	II1
6	2001.83	87.9	1.1	5.5	5.5	78.8	II1
7	2003.73	83.5	1.0	12.4	3.1	71.6	II1
8	2009.67	86.4	1.7	6.8	5.1	77.1	II1
9	2011.9	87.5	1.3	6.3	5.0	78.4	II1
10	2014.61	86.2	1.7	6.9	5.2	76.7	II1
11	2016.19	87.2	1.1	6.4	5.3	77.7	II1
12	2017.79	88.8	1.3	5.0	5.0	80.6	I
15	2033.26	88.9	1.1	6.7	3.3	81.1	I
16	2035.55	86.7	1.1	6.7	5.6	76.7	II1
17	2038.03	88.2	1.2	5.9	4.7	79.7	II1
18	2042.78	81.6	1.3	9.2	7.9	67.4	II1
20	2046.54	80.6	1.0	7.1	11.2	64.5	II1
22	2051.29	83.7	1.1	7.6	7.6	70.9	II1
24	2062.55	85.1	1.1	8.5	5.3	73.9	II1

The type index of organic matter (TI) = (sapropelinite \times 100 + liptinite \times 50 - vitrinite \times 75 - inertinite \times 100)/100.

4.2.3. Maturity

Ro and T_{max} are extensively used to characterize the maturity of organic matter [23]. Ro values were measured for all twenty-four shale samples (Table 2). The shale samples from the Qingshankou Formation had an Ro between 1.01 and 1.12 (on average 1.07), suggesting that organic matter in Qingshankou lacustrine shales samples was in a mature stage (Table 2). T_{max} values range from 435 °C and 459 °C, and averaged 449 °C (Table 2, Figure 5), indicating the thermal evolution of the Qingshankou shale samples fall in oil window.

4.3. Paleoenvironment

4.3.1. Sources of Organic Matter

Organic matter in source rock comes from a variety of sources, including endogenous lower organisms and allochthonous continental organic matter, which can be reflected by biomarker combinations of hydrocarbons generated by them [23,37–40]. Specific biomarker parameters and their combinations can be used to quantitatively reflect relative contributions of specific types of organisms.

Distribution features of chain alkanes can characterize the organic source and maturity of organic matter [23,37]. Ratios of some normal alkanes can reflect the variations of relative abundances of continental and aquatic organisms. Immature source rocks with organic matter dominated by continental plants generate hydrocarbons with more molecules with odd numbers that are particularly carbon rich in *n*-C27, *n*-C29, and *n*-C31. These *n*-alkanes from epidermal keratinine wax were compounded by higher plants directly or from alcohol or ester compounds with even carbon numbers losing functional groups, while *n*-C24 to *n*-C25 originated coming from marine organic matter.

Generally, the values of carbon preference index(CPI) decrease with a growth in maturity, and this is attributed to the mixing of *n*-alkanes generated by kerogen composed of different organism precursors and normal alkanes generated by hydrocarbon cracking in the early diagenetic stage. Hence, a high CPI generally implies low maturity and input from continental plants, while source rock with a CPI of around 1 have dominant marine input and high maturity [41,42]. The shale samples have a CPI between 1.01 and 1.20 (1.11 on average, Table 2), indicating Qingshankou lacustrine shales has relatively high organic matter maturity.

Organic matter input and sedimentary conditions have a strong impact on biomarkers in extractions from the source rock. Since C₂₇ sterols derive mainly from plankton, C₂₈ sterols from phytoplankton, and C₂₉ sterols are abundant in land plants, the relative abundance of C₂₇ααα(20R), C₂₈ααα(20R) and C₂₉ααα(20R) regular steranes is often used to determine the dominant source of OM [38,43,44]. The Qingshankou lacustrine shale samples have relative contents of C₂₇, C₂₈, and C₂₉ regular sterane of 26.52–35.17% (30.54% on average), 19.88–28.13% (22.88% on average), and 41.69–52.34% (46.58% on average), respectively (Table 2). Figure 8 shows that all the shale samples fall in the plankton/bacterial and plankton/land plant fields. Thus, the organic matter in the Qingshankou shale samples is mainly from a mixture of plankton, bacterial and land plants.

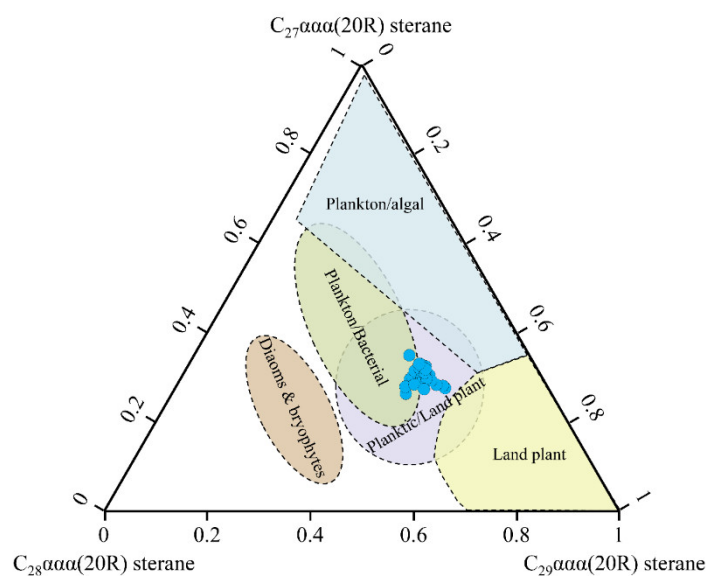


Figure 8. Ternary diagram of C₂₇, C₂₈, and C₂₉ regular steranes showing the relationship.

4.3.2. Redox Environment

Water salinity affects the flourishing of aquatic organisms such as algae and, in turn, the input of organic matter. The water redox condition determines if the organic matter can be preserved effectively [45–47]. Suitable water salinity is conducive to the growth and reproduction of algae, which in turn affects the lake's productivity. In some cases, increased nutrient inputs and optimal redox conditions could cause algal bloom in freshwater environments [48–50].

Under a certain salinity range, with the increase in salinity, algae growth gradually flourished, forming higher productivity and good preservation condition. However, over a certain salinity range, the algae are inhibited in growth and even do not develop at all [46]. An oxidizing water body can promote the reproduction of bacteria, leading to the massive consumption of organic matter in the sediment; on the other hand, in a reducing environment with suitable salinity, the reproduction of bacteria is inhibited, so the organic matter deposited can be preserved well.

Gammacerane/ C_{30} hopane ($G/C_{30}H$) is a parameter commonly used to characterize the salinity of a sedimentary environment [37,51]. It is generally believed that $G/C_{30}H > 0.11$ indicates a reducing water environment [52]. As shown in Table 2, the shale samples from the Qingshankou Formation have $G/C_{30}H$ values between 0.31 and 0.65 (0.42 on average), suggesting that Qingshankou's lacustrine shales formed in reducing saline water (Figure 9).

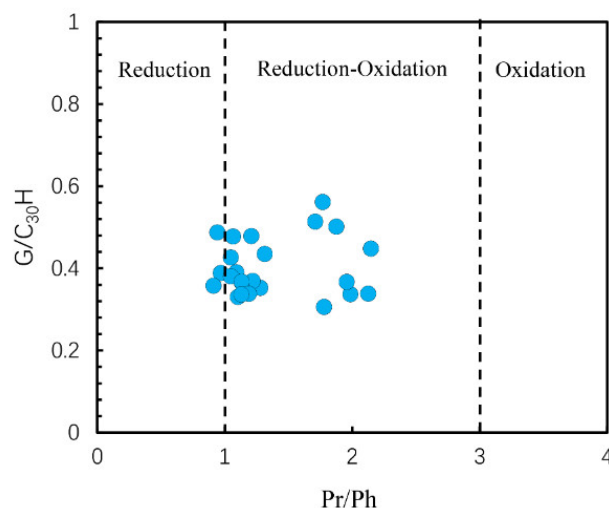


Figure 9. Diagram of $G/C_{30}H$ vs. Pr/Ph .

Pristane/phytane (Pr/Ph) is a classic parameter for identifying redox conditions [53,54]. A Pr/Ph of less than 1, 1–3, and more than 3 indicates reducing, weakly reducing, and oxidizing conditions, respectively. However, some researchers hold that organic matter maturity affects Pr/Ph , which should be kept in mind when judging the sedimentary environment of organic matter by Pr/Ph [55–57]. It can be seen from the diagram of Pr/Ph vs. T_{max} (Figure 10) that they have no significant correlation, which means that Pr/Ph is not affected by the thermal evolution degrees of organic matter, thus Pr/Ph can be used to identify the sedimentary environment. As shown in Table 2, the shale samples from the Qingshankou Formation have Pr/Ph values between 0.71 and 1.32 (1.03 on average), indicating that the organic matter in shale samples was formed in a reducing–weakly reducing sedimentary environment. The $Ph/n-C_{18}$ and $Pr/n-C_{17}$ ratio of the saturated hydrocarbon vary from 0.10 to 0.21 (average: 0.15) and 0.01 and 0.26 (average: 0.16), respectively. Figure 11 shows that the Qingshankou lacustrine shales samples were from a mixture of organic matter and formed in a semi-oxidation and semi-reduction environment (Figure 11).

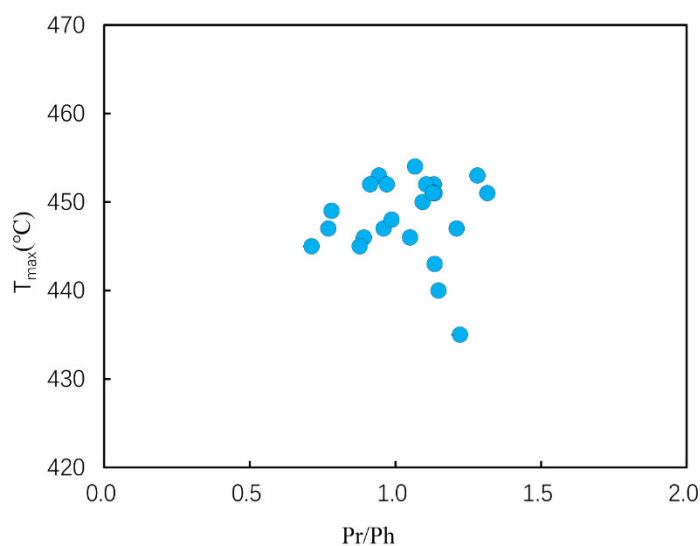


Figure 10. Diagram of Pr/Ph and T_{\max} .

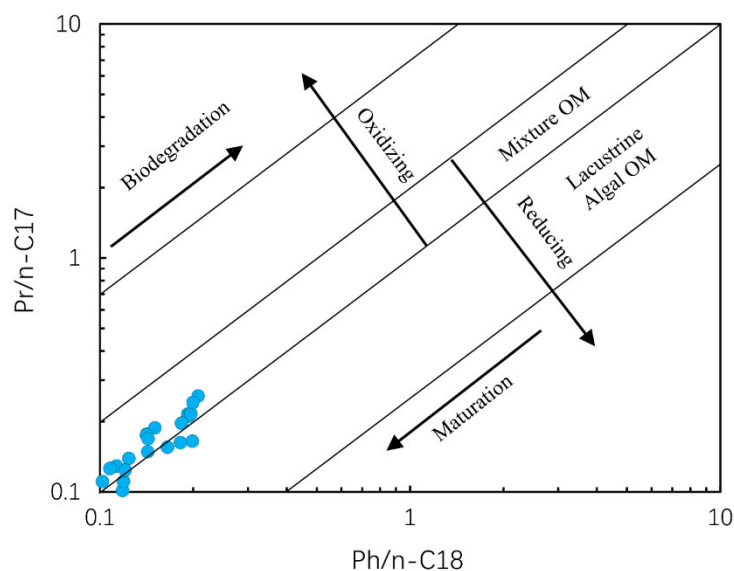


Figure 11. Diagram of Pr/ n -C₁₇ vs. Ph/ n -C₁₈ of the shale samples, showing redox conditions and organic matter sources (Adapted from Refs. [58,59]), OM = Organic matter.

5. Conclusions

(1) Lacustrine shale samples from the Qingshankou Formation of southern Songliao Basin have high organic matter abundances, reaching the standard of a “good” and “excellent” source rock, types I and II kerogen, with oil-generation potential, and in a mature stage of organic matter.

(2) The origin of the organic matter in Qingshankou shale samples were mainly from a mixture of plankton, bacterial and land plants.

(3) The shale samples were formed in a semi-oxidation and semi-reduction environment, which is conducive to the preservation of organic matter.

Author Contributions: Data curation, Z.L., Z.B. and Z.W.; Formal analysis, Z.L.; Funding acquisition, Z.L., Z.B. and H.W.; Methodology, Z.L. and H.W.; Software, L.L.; Visualization, H.W. All authors have read and agreed to the published version of the manuscript.

Funding: The authors thank the support from PETROCHINA (Grant Nos. 2021DJ0203, 2021DJ0205, and 2021DJ2207).

Institutional Review Board Statement: Not applicable.

Informed Consent Statement: Not applicable.

Data Availability Statement: Data are available from the authors upon request.

Acknowledgments: The authors would like to express their gratitude to the PetroChina Jilin Oilfield Company for providing the resources required to collect the samples used in this study. We also acknowledge the precious advice of the editors and reviewers.

Conflicts of Interest: The authors declare no conflict of interest.

References

1. Newport, L.; Aplin, A.; Gluyas, J. Geochemical and lithological controls on a potential shale reservoir: Carboniferous Holywell Shale, Wales. *Mar. Pet. Geol.* **2016**, *71*, 198–210. [\[CrossRef\]](#)
2. Wang, M.; Guo, Z.; Jiao, C. Exploration progress and geochemical features of lacustrine shale oils in China. *J. Pet. Sci. Eng.* **2019**, *178*, 975–986. [\[CrossRef\]](#)
3. Li, J.; Lu, S.; Zhang, J.; Zhang, P.; Xue, H. Quantitative evaluation models of adsorbed and free shale oil and its microscopic occurrence mechanism. *Oil Gas Geol.* **2019**, *40*, 583–592.
4. Bechtel, A.; Jia, J.; Strobl, S.; Sachsenhofer, R.F. Palaeoenvironmental conditions during deposition of the Upper Cretaceous oil shale sequences in the Songliao Basin (NE China): Implications from geochemical analysis. *Org. Geochem.* **2012**, *46*, 76–95. [\[CrossRef\]](#)
5. Fan, X.; Su, J.Z.; Chang, X.; Huang, Z.W.; Zhou, T.; Guo, Y.T.; Wu, S.Q. Brittleness evaluation of the inter-salt shale oil reservoir in Jiangnan Basin in China. *Mar. Pet. Geol.* **2018**, *102*, 109–115. [\[CrossRef\]](#)
6. Liu, B.; Sun, J.; Zhang, Y.; He, J.; Fu, X.; Yang, L.; Xing, J.; Zhao, X. Reservoir space and enrichment model of shale oil in the first member of Cretaceous Qingshankou Formation in the Changling Sag, southern Songliao Basin, NE China. *Pet. Explor. Dev.* **2021**, *48*, 17. [\[CrossRef\]](#)
7. Wang, Z.; Tang, Y.; Wang, Y. Kinetics of shale oil generation from kerogen in saline basin and its exploration significance: An example from the Eocene Qianjiang Formation, Jiangnan Basin, China—ScienceDirect. *J. Anal. Appl. Pyrolysis* **2020**, *150*, 104885. [\[CrossRef\]](#)
8. Xu, J.; Liu, Z.; Bechtel, A.; Sachsenhofer, R.; Jia, J.; Meng, Q.; Sun, P. Organic matter accumulation in the Upper Cretaceous Qingshankou and Nenjiang Formations, Songliao Basin (NE China): Implications from high-resolution geochemical analysis. *Mar. Pet. Geol.* **2019**, *102*, 187–201. [\[CrossRef\]](#)
9. Katz, B. Controls on distribution of lacustrine source rocks through time. *AAPG* **1990**, *50*, 132–139.
10. Neumann, V.; Borrego, A.; Cabrera, L.; Dino, R. Organic matter composition and distribution through the Aptian–Albian lacustrine sequences of the Araripe Basin, northeastern Brazil. *Int. J. Coal Geol.* **2003**, *54*, 21–40. [\[CrossRef\]](#)
11. He, T.; Li, W.; Lu, S.; Yang, E.; Jing, T.; Ying, J.; Zhu, P.; Wang, X.; Pan, W.; Zhang, B.; et al. Quantitatively unmixing method for complex mixed oil based on its fractions carbon isotopes: A case from the Tarim Basin, NW China. *Pet. Sci.* **2022**, *in press*. [\[CrossRef\]](#)
12. Wei, H.; Chen, D.; Wang, J.; Yu, H.; Tucker, M. Organic accumulation in the lower Chihshia Formation (Middle Permian) of South China: Constraints from pyrite morphology and multiple geochemical proxies. *Palaeogeogr. Palaeoclimatol. Palaeoecol.* **2012**, *353–355*, 73–86. [\[CrossRef\]](#)
13. Cao, H.; Kaufman, A.; Shan, X.; Cui, H.; Zhang, G. Sulfur isotope constraints on marine transgression in the lacustrine Upper Cretaceous Songliao Basin, northeastern China. *Palaeogeogr. Palaeoclimatol. Palaeoecol.* **2016**, *451*, 152–163. [\[CrossRef\]](#)
14. Ding, X.; Liu, G.; Zha, M. Characteristics and origin of lacustrine source rocks in the Lower Cretaceous, Erlian Basin, northern China. *Mar. Pet. Geol.* **2015**, *66*, 939–955. [\[CrossRef\]](#)
15. Jones, M.; Ibarra, D.; Gao, Y.; Sageman, B.; Selby, D.; Chamberlain, C.; Graham, S. Evaluating Late Cretaceous OAEs and the influence of marine incursions on organic carbon burial in an expansive East Asian paleo-lake. *Earth Planet. Sci. Lett.* **2018**, *484*, 41–52. [\[CrossRef\]](#)
16. Tong, X.; Hu, J.; Xi, D.; Zhu, M.; Song, J.; Peng, P. Depositional environment of the Late Santonian lacustrine source rocks in the Songliao Basin (NE China): Implications from organic geochemical analyses. *Org. Geochem.* **2018**, *124*, 215–227. [\[CrossRef\]](#)
17. Wang, Y.; Deng, S.W.; Fan, J.; Zou, X.P.; Yang, J. Natural gas geology, resource potential and favorable exploration direction in the south of Songliao Basin. *Nat. Gas Geosci.* **2018**, *29*, 1455–1464.
18. Li, Z.; Bao, Z.; Wei, Z.; Wang, H.; Zhao, W.; Dong, W.; Shen, Z.; Wu, F.; Tian, W.; Li, L. Characteristics and Affecting Factors of K 2 qn 1 Member Shale Oil Reservoir in Southern Songliao Basin, China. *Energies* **2022**, *15*, 2269. [\[CrossRef\]](#)
19. Wu, Y.; Lu, Y.; Jiang, S. Pore structure characterization of different lithofacies in marine shale: A case study of the Upper Ordovician Wufeng-Lower Silurian Longmaxi formation in the Sichuan Basin, SW China. *J. Nat. Gas Sci. Eng.* **2018**, *57*, 203–215. [\[CrossRef\]](#)
20. Guo, X.; Qin, Z.; Yang, R. Comparison of pore systems of clay-rich and silica-rich gas shales in the lower Silurian Longmaxi formation from the Jiaoshiba area in the eastern Sichuan Basin, China. *Mar. Pet. Geol.* **2019**, *101*, 265–280. [\[CrossRef\]](#)

21. Xu, S.; Gou, Q.; Hao, F. Shale pore structure characteristics of the high and low productivity wells, Jiaoshiba shale gas field, Sichuan Basin, China: Dominated by lithofacies or preservation condition? *Mar. Pet. Geol.* **2020**, *114*, 104211. [[CrossRef](#)]
22. Baban, D. Sedimentary organic matter and source rock potential of the Paleocene Aaliji Formation in Qumar Oil Field, NE Iraq. *Arab. J. Geosci.* **2014**, *7*, 4733–4744. [[CrossRef](#)]
23. Tissot, B.; Welte, D. *Petroleum Formation and Occurrence*; Springer: Berlin/Heidelberg, Germany; New York, NY, USA, 1984.
24. Peters, K.; Cassa, M. *Applied Source Rock Geochemistry: Chapter 5: Part II. Essential Elements*; AAPG: Houston, TX, USA, 1994; pp. 93–120.
25. Wang, M.; Wilkins, R.; Song, G. Geochemical and geological characteristics of the Es3L lacustrine shale in the Bonan sag, Bohai Bay Basin, China. *Int. J. Coal Geol.* **2015**, *138*, 16–29. [[CrossRef](#)]
26. He, T.; Li, W.; Lu, S.; Yang, E.; Jing, T.; Ying, J.; Zhu, P.; Wang, X.; Pan, W.; Chen, Z. Distribution and isotopic signature of 2-alkyl-1,3,4-trimethylbenzenes in the Lower Paleozoic source rocks and oils of Tarim Basin: Implications for the oil-source correlation. *Pet. Sci.* **2022**, in press. [[CrossRef](#)]
27. John, M. Generation of gas and oil from coal and other terrestrial organic matter. *Org. Geochem.* **1991**, *17*, 673–680.
28. Karayigit, A.; Oskay, R.; Elik, Y. Mineralogy, petrography, and Rock-Eval pyrolysis of late Oligocene coal seams in the Malkara coal field from the Thrace Basin (NW Turkey). *Int. J. Coal Geol.* **2021**, *244*, 103814. [[CrossRef](#)]
29. Pepper, A.; Corvi, P. Simple kinetic models of petroleum formation. Part I: Oil and gas generation from kerogen. *Mar. Pet. Geol.* **1995**, *12*, 291–319. [[CrossRef](#)]
30. Yang, S.; Horsfield, B. Critical review of the uncertainty of Tmax in revealing the thermal maturity of organic matter in sedimentary rocks. *Int. J. Coal Geol.* **2020**, *225*, 103500. [[CrossRef](#)]
31. Vu, T.; Horsfield, B.; Mahlstedt, N.; Schenk, H.; Kelemen, S.; Walters, C.; Kwiatek, P.; Sykes, R. The structural evolution of organic matter during maturation of coals and its impact on petroleum potential and feedstock for the deep biosphere. *Org. Geochem.* **2013**, *62*, 17–27. [[CrossRef](#)]
32. Carvajal-Ortiz, H.; Gentzis, T. Geochemical screening of source rocks and reservoirs: The importance of using the proper analytical program. *Int. J. Coal Geol.* **2018**, *190*, 56–69. [[CrossRef](#)]
33. Sanei, H.; Petersen, H.; Schovsbo, N.; Jiang, C.; Goodsite, M. Petrographic and geochemical composition of kerogen in the Furongian (U. Cambrian) Alum Shale, central Sweden: Reflections on the petroleum generation potential. *Int. J. Coal Geol.* **2014**, *132*, 158–169. [[CrossRef](#)]
34. Cornford, C.; Gardner, P.; Burgess, C. Geochemical truths in large data sets. I: Geochemical screening data. *Org. Geochem.* **1998**, *29*, 530. [[CrossRef](#)]
35. Liu, B.; Mastalerz, M.; Schieber, J. SEM petrography of dispersed organic matter in black shales: A review. *Earth-Sci. Rev.* **2022**, *224*, 103874. [[CrossRef](#)]
36. Hackley, P.C.; Cardott, B.J. Application of organic petrography in North American shale petroleum systems: A review. *Int. J. Coal Geol.* **2016**, *163*, 8–51. [[CrossRef](#)]
37. Peters, K.E.; Moldowan, J. *The Biomarker Guide: Interpreting Molecular Fossils in Petroleum and Ancient Sediments*; Prentice Hall: Englewood Cliffs, NJ, USA, 1993.
38. Peters, K.; Walters, C.; Moldowan, J. *The Biomarker Guide: Biomarkers and Isotopes in Petroleum Systems and Earth History*; Cambridge University Press: Cambridge, UK, 2004.
39. Seifert, W.; Moldowan, J. Use of biological markers in petroleum exploration. *Methods Geochem.* **1986**, *24*, 261–290.
40. He, T.; Li, W.; Lu, S.; Pan, W.; Sun, D. Mechanism and geological significance of anomalous negative $\delta^{13}\text{C}$ kerogen in the Lower Cambrian, NW Tarim Basin, China. *J. Pet. Sci. Eng.* **2021**, *208*, 109384. [[CrossRef](#)]
41. Bray, E.; Evans, E. Distribution of n-paraffins as a clue to recognition of source beds. *Geochim. Cosmochim. Acta* **1961**, *22*, 2–15. [[CrossRef](#)]
42. Scalan, E.; Smith, J.E. An improved measure of the odd-even predominance in the normal alkanes of sediment extracts and petroleum. *Geochim. Cosmochim. Acta* **1970**, *34*, 611–620. [[CrossRef](#)]
43. Bhattacharya, S.; Dutta, S.; Summons, R. A distinctive biomarker assemblage in an Infracambrian oil and source rock from western India: Molecular signatures of eukaryotic sterols and prokaryotic carotenoids. *Precambrian Res.* **2016**, *290*, 101–112. [[CrossRef](#)]
44. Huang, W.; Meinschein, W. Sterols as ecological indicators. *Geochim. Cosmochim. Acta* **1979**, *43*, 739–745. [[CrossRef](#)]
45. Hao, F.; Zhou, X.; Zhu, Y.; Yang, Y. Lacustrine source rock deposition in response to co-evolution of environments and organisms controlled by tectonic subsidence and climate, Bohai Bay Basin, China. *Org. Geochem.* **2012**, *42*, 323–339. [[CrossRef](#)]
46. He, T.; Lu, S.; Li, W.; Tan, Z.; Zhang, X. Effect of Salinity on Source Rock Formation and Its Control on the Oil Content in Shales in the Hetaoyuan Formation from the Biyang Depression, Nanxiang Basin, Central China. *Energy Fuels* **2018**, *32*, 6698–6707. [[CrossRef](#)]
47. Li, W.; Lu, S.; Tan, Z.; He, T. Lacustrine Source Rock Deposition in Response to Co-evolution of Paleoenvironment and Formation Mechanism of Organic-rich Shales in the Biyang De-pression, Nanxiang Basin. *Energy Fuels* **2017**, *31*, 13519–13527. [[CrossRef](#)]
48. Celik, Y.; Karayigit, A.; Oskay, R.; Zer, M. A multidisciplinary study and palaeoenvironmental interpretation of middle Miocene Keles lignite (Harmanck Basin, NW Turkey), with emphasis on syngenetic zeolite formation. *Int. J. Coal Geol.* **2021**, *237*, 103691. [[CrossRef](#)]

49. Bai, Y.; Liu, Z.; George, S.; Meng, J. A Comparative Study of Different Quality Oil Shales Developed in the Middle Jurassic Shimengou Formation, Yuqia Area, Northern Qaidam Basin, China. *Energies* **2022**, *15*, 1231. [[CrossRef](#)]
50. Warwick, P.; Hook, R. Petrography, geochemistry, and depositional setting of the San Pedro and Santo Tomas coal zones: Anomalous algae-rich coals in the middle part of the Claiborne Group (Eocene) of Webb County, Texas. *Int. J. Coal Geol.* **1995**, *28*, 303–342. [[CrossRef](#)]
51. Moldowan, J.; Sundararaman, P.; Schoell, M. Sensitivity of biomarker properties to depositional environment and/or source input in the Lower Toarcian of SW-Germany. *Org. Geochem.* **1986**, *10*, 915–926. [[CrossRef](#)]
52. Damsté, J.; Kenig, F.; Koopmans, M. Evidence for gammacerane as an indicator of water column stratification. *Geochim. Cosmochim. Acta* **1995**, *59*, 1895. [[CrossRef](#)]
53. Didyk, B.; Simoneit, B.; Brassell, S.; Eglinton, G. Organic geochemical indicators of palaeoenvironmental conditions of sedimentation. *Nature* **1978**, *272*, 216–222. [[CrossRef](#)]
54. Mello, M.; Telnaes, N.; Gaglianone, P.; Chicarelli, M.; Brassell, S.; Maxwell, J. Organic geochemical characterisation of depositional palaeoenvironments of source rocks and oils in Brazilian marginal basins. *Org. Geochem.* **1988**, *13*, 31–45. [[CrossRef](#)]
55. Chen, D.; Pang, X.; Li, L.; Jiang, F.; Han, W. Organic geochemical characteristics and shale oil potential of the middle Eocene early-mature shale in the Nanpu Sag, Bohai Bay Basin, Eastern China. *Mar. Pet. Geol.* **2021**, *4*, 105248. [[CrossRef](#)]
56. Ten, H.; De Leeuw, J.; Rullk, T.; Damsté, J. Restricted utility of the pristane/phytane ratio as a palaeoenvironmental indicator. *Nature* **1987**, *330*, 641–643.
57. Zhou, W.; Zheng, Y.; Meyers, P.; Jull, A.; Xie, S. Postglacial climate-change record in biomarker lipid compositions of the Hani peat sequence, Northeastern China. *Earth Planet. Sci. Lett.* **2010**, *294*, 37–46. [[CrossRef](#)]
58. Shanmugam, G. Significance of coniferous rain forests and related organic matter in generating commercial quantities of oil, Gippsland Basin, Australia. *AAPG Bull.* **1985**, *69*, 1241–1254. [[CrossRef](#)]
59. Si, W.; Hou, D.; Wu, P.; Zhao, Z.; Cao, L. Geochemical characteristics of lower cretaceous lacustrine organic matter in the southern sag of the Wuliyasitai depression, Erlian Basin, China. *Mar. Pet. Geol.* **2020**, *118*, 104404. [[CrossRef](#)]